Applied Thermal Engineering 93 (2016) 529–536

Contents lists available at ScienceDirect

Applied Thermal Engineering

journal homepage: www.elsevier.com/locate/apthermeng

Research Paper

A space-fractional model of thermo-electromagnetic wave propagation in anisotropic media

F.A. Godínez [a], O. Chávez [b], A. García [c], R. Zenit [d,*]

[a] Instituto de Ingeniería, Universidad Nacional Autónoma de México, Apdo. Postal 70-360, Ciudad Universitaria, D.F. 04510, Mexico
[b] División de Estudios de Posgrado e Investigación, Instituto Tecnológico de Chihuahua, Avenida Tecnológico 2909, Chihuahua, Mexico
[c] Tecnología Aplicada en Exploración y Producción Petrolera, Inc., Homero 714, Polanco, D.F. 11560, Mexico
[d] Instituto de Investigaciones en Materiales, Universidad Nacional Autónoma de México, Apdo. Postal 70-360, Ciudad Universitaria, D.F. 04510, Mexico

HIGHLIGHTS

- A conjugate theoretical model was developed to study the heat propagation in fractal media.
- The model couples electromagnetic and thermal conservation equations in fractal space.
- Solutions of the model are obtained numerically in dimensionless terms.
- A maximum heat transfer rate is observed at an intermediate fractal dimension.

ARTICLE INFO

Article history:
Received 24 June 2015
Accepted 29 September 2015
Available online 22 October 2015

Keywords:
Thermo-electromagnetic
Complex porous media
Fractional model

ABSTRACT

A theoretical study of the propagation of electromagnetic waves through anisotropic media is presented. A Euclidean nonlinear model that couples Maxwell's and heat transfer equations is generalized considering Stillinger's formalism in terms of a spatial fractal dimension α. The numerical results reveal a significant influence of α on current density and temperature distributions along the radial direction of a cylindrical conductor. When α increases approaching unity, the anisotropy of the medium becomes increasingly weak; thus the wave penetrates deeper into the medium and the skin effect is weakened. Interestingly, the steady state temperature at any location along the radial direction reaches a maximum at $\alpha = 1/2$. Beyond this maximum, the temperature decreases with increasing α, reaching a finite value at the Euclidean limit $\alpha = 1$. The generalized model presented here not only simplifies the analysis of electromagnetic transmission through complex structures such as porous media but also provides a quantitative measure of the anisotropy along the radial direction of the conductive medium by a fractional dimension.

1. Introduction

Fractional calculus is a generalization of ordinary differentiation and integration to arbitrary non-integer order. This concept is as old as the integer-order calculus originally developed by Newton and Leibniz in the 17th century [1]. Although fractional calculus has a long history, in recent decades it has attracted the interest of researchers in diverse areas of engineering and science. The fractional calculus and in particular the fractional differential equations are used to describe complex systems with "memory" in time and/or space domains [2,3]. Usually these memory effects are modeled via non-local integro-differential operators as those studied by Riemann-Liouville [4], Caputo [5] and Grünwald-Letnikov [6] for time domain; and Riesz [6–8] as well as Caputo [3] for space domain. The non-local property of these operators can be used to construct simple material models and unified principles [9]. Interesting examples of diffusion processes can be found in [10,11]; examples of modeling viscoelastic materials have been reported by [5,12], and applications in the field of signal processing are discussed in [13]. Various problems of electromagnetic theory using concepts of fractional calculus have been investigated by some researchers [6,14,15]. Particularly, the study of wave propagation and scattering in fractal structures is important in practical applications such as communications, remote sensing and navigation [16], and the microstructural characterization of rocks for estimating oil reserves [17]. This paper deals with the application of the concept of fractional space to theoretically investigate the transmission of electromagnetic waves through anisotropic media such as some porous materials. This issue has been addressed recently in a series of articles by Zubair et al. [18–21] in which the electromagnetic transmission is analyzed for different coordinate systems. The novelty of our approach is that it takes into account two effects during wave propagation: the Joule heating effect [22] and the well-known skin effect observed in conductors [23]. The basis for the analysis is a

* Corresponding author. Tel.: +525556224593; fax: +52 55 5622 4602.
E-mail address: zenit@unam.mx (R. Zenit).

http://dx.doi.org/10.1016/j.applthermaleng.2015.09.119
1359-4311/

recently developed model which couples Maxwell's equations with the heat transfer equation in a Euclidean space to simulate electromagnetic wave propagation through a biphasic medium [24]. Then, these equations are re-derived for fractional space by using the Stillinger formalism [25]. The physics behind this mathematical formalism is to replace a real anisotropic solid (confining structure) with an isotropic system in a D-dimensional fractional space, where the measure of the anisotropy or confinement of the solid is given by the value of D [26–28]. Thus, when the value of D is given, the real system can be tackled numerically by using conventional finite-difference schemes. The paper is organized as follows. In Section 2 we describe the physical model under study. Furthermore, the thermo-electromagnetic models in Euclidean and fractional space as well as the numerical scheme for calculations are introduced. In Section 3 numerical results are presented. Finally, some concluding remarks and discussions are drawn in Section 4.

2. Description of the phenomenon

The physical model under study is shown in Fig. 1. We consider a cylindrical electrical conductor composed of an anisotropic medium with constant physical properties. This conductor has a length L and the conductive phase is bounded at a radius R. A sudden flow of alternating electric current through this conductor is established. Thus, a rise of temperature is originated as a result of the electric current, causing the well-known Joule's effect. For large values of the frequency associated with the alternating current, a redistribution of the current density is inevitable and the skin effect yields a tendency of the electric current to flow over the surface of the conductor.

2.1. The thermo-electromagnetic model in Euclidean space

A thermo-electromagnetic model in a Euclidean space was developed by [24] to analyze simultaneously the conjugate heat conductive mechanism resulting from an alternating electrical current that flows continuously through a cylindrical bimetallic conductor (two conducting phases), assuming that the electric resistivity of both phases is linearly dependent on temperature. This model couples Maxwell's equations with the heat conduction equation which includes a heat source due to Joule's effect. Please note that for this model the other physical properties are assumed to remain constant; clearly, this is not the case. We could, in principle, add other laws of dependence with temperature without much more difficulty. However, we chose to address this simplified case to isolate the effect of the electric conductivity because it is the dominant mechanism in this problem.

The following are the equations for one conducting phase assuming only temperature, T, and density current, J_s, variations in the radial coordinate r (see definition of all variables in the Nomenclature):

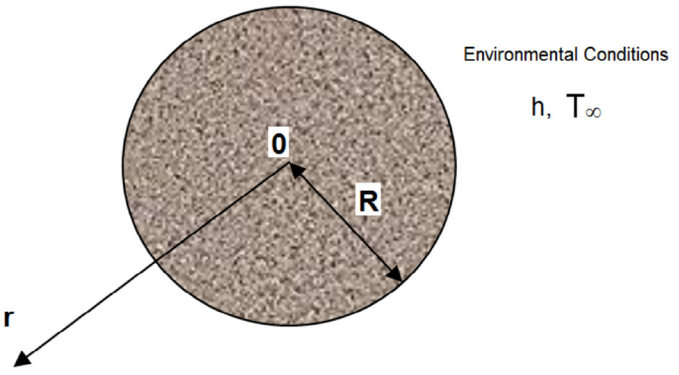

Fig. 1. The physical model of the considered conductor.

$$\frac{d^2J_s}{dr^2}+\left(\frac{2\phi}{1+\phi(T-T_\infty)}\frac{\partial T}{\partial r}+\frac{1}{r}\right)\frac{dJ_s}{dr}+\frac{\phi}{1+\phi(T-T_\infty)}\left[\frac{\partial^2T}{\partial r^2}+\frac{1}{r}\frac{\partial T}{\partial r}\right]J_s=\frac{2i}{\delta^2}J_s \tag{1}$$

and

$$\frac{k}{r}\frac{\partial}{\partial r}\left(r\frac{\partial T}{\partial r}\right)+\lambda_\infty[1+\phi(T-T_\infty)]|J_s|^2=(\rho c)\frac{\partial T}{\partial t} \tag{2}$$

This system is subjected to the boundary conditions:

$$\text{at}\quad r=0:\quad J_s=\text{finite},\quad T=\text{finite} \tag{3}$$

$$\text{at}\quad r=R:\quad J_s=J_R,\quad -k_E\frac{\partial T}{\partial r}=h(T-T_\infty) \tag{4}$$

and to the initial condition,

$$t=0:\quad T=T_\infty. \tag{5}$$

J_R, the current density at the surface of the conductor, is restricted to satisfy the following condition:

$$I_{tot}=2\pi\int_0^R J_s\,r dr. \tag{6}$$

In the above equations, the subscript "s" denotes the spatial dependence of the current density $\bar{J}(r,t)$, which is considered as $\bar{J}=J_s(r)e^{i\omega t}$. Furthermore, we have introduced in Eq. (1) the conductor skin depth parameter [28] given by $\delta=(2\lambda/\omega\mu)^{1/2}$.

On the other hand, the linear relationship between the electrical resistivity and the temperature is given by $\lambda=\lambda_\infty[1+\phi(T-T_\infty)]$. This assumption is frequently used in literature; its validity depends on the type of conductor materials and the temperature range at which the thermo-electrical transmission occurs [29,30]. Again, please refer to Nomenclature for the definition of all variables.

2.2. The thermo-electromagnetic model in fractional-dimensional space

A cylindrical coordinate system of the space-fractional Laplacian operator is defined as [18]:

$$\nabla^2=\frac{\partial^2}{\partial^2 r}+\frac{1}{r}(\alpha_1+\alpha_2-1)\frac{\partial}{\partial r}+\frac{1}{r^2}\left(\frac{\partial^2}{\partial\Phi^2}-\{(\alpha_1-1)tan\Phi-(\alpha_2-1)cot\Phi\}\frac{\partial}{\partial\Phi}\right)+\frac{\partial^2}{\partial z^2}+\frac{\alpha_3-1}{z}\frac{\partial}{\partial z}, \tag{7}$$

where the α-parameters ($0<\alpha_1\le 1, 0<\alpha_2\le 1$ and $0<\alpha_3\le 1$) describe the distribution of space in each coordinate independently. The total spatial dimension of the system is $D=\alpha_1+\alpha_2+\alpha_3$ [31].

In this study only the variations of the temperature and current density in the radial direction are considered. Therefore, the derivatives with respect to Φ and z coordinates are assumed to be zero. Furthermore, if we set $\alpha_2=1$ and $\alpha_3=1$, the Laplacian operator (7) becomes:

$$\nabla^2=\frac{1}{r^{\alpha_1}}\frac{\partial}{\partial r}\left(r^{\alpha_1}\frac{\partial}{\partial r}\right)=\frac{\partial^2}{\partial r^2}+\frac{\alpha_1}{r}\frac{\partial}{\partial r},\quad 0<\alpha_1\le 1, \tag{8}$$

or equivalently

$$\nabla^2=\frac{1}{r^{D-2}}\frac{\partial}{\partial r}\left(r^{D-2}\frac{\partial}{\partial r}\right)=\frac{\partial^2}{\partial r^2}+\frac{D-2}{r}\frac{\partial}{\partial r},\quad 0<\alpha_1\le 1. \tag{9}$$

For simplicity, we will use from now on the Laplacian defined by Eq. (8). In order to reduce the number of physical parameters of the proposed model, the following dimensionless variables and parameters are introduced:

$$\theta=\frac{T-T_\infty}{\Delta T_c},\quad \tau=\frac{tk}{(\rho c)R^2},\quad \eta=\frac{r}{R},\quad Bi=\frac{hb}{k_r},$$

$$\varphi=\frac{J_s}{J_R},\quad \kappa=\phi\Delta T_c,\quad \Delta T_c=\frac{\lambda_\infty J_R^2 R^2}{k},\quad \varepsilon=\frac{\delta}{R}. \tag{10}$$

Substituting Eqs. (8) and (10) into Eqs. (1) and (2), we can obtain the dimensionless thermo-electromagnetic model in fractional space:

$$\frac{d^2\varphi}{d\eta^2}+\left(\frac{2\kappa}{1+\kappa\theta}\frac{\partial\theta}{\partial\eta}+\frac{\alpha_1}{\eta}\right)\frac{d\varphi}{d\eta}+\frac{\kappa}{1+\kappa\theta}\left[\frac{\partial^2\theta}{\partial\eta^2}+\frac{\alpha_1}{\eta}\frac{\partial\theta}{\partial\eta}\right]\varphi=\frac{2i}{(1+\kappa\theta)\varepsilon^2}\varphi, \tag{11}$$

$$\frac{\partial^2\theta}{\partial\eta^2}+\frac{\alpha_1}{\eta}\frac{\partial\theta}{\partial\eta}+(1+\kappa\theta)|\varphi|^2=\frac{\partial\theta}{\partial\tau}. \tag{12}$$

These equations are solved, subjected to the following boundary conditions:

$$\text{at}\quad \eta=0:\quad \varphi=\text{finite},\quad \theta=\text{finite} \tag{13}$$

$$\text{at}\quad \eta=1:\quad \varphi=1,\quad \frac{\partial\theta}{\partial\eta}=-Bi\theta \tag{14}$$

and to the initial condition,

$$\tau=0:\quad \theta=0. \tag{15}$$

Note that when substituting $\alpha_1=1$ into Eqs. (11) and (12), the thermo-electromagnetic model in the Euclidean space is recovered. The system of equations defined by the set (11)–(15) is influenced by three parameters: κ, ε and α_1. For the sake of notational simplicity, the parameter α_1 is henceforth replaced just with α. The dimensionless parameters ε and κ are introduced to quantify the electrical thickness of the current density and the level of coupling between both electromagnetic (11) and thermal (12) models, respectively. The parameter α describes the degree of anisotropy of the medium in the radial direction [26].

2.3. Numerical scheme

The above dimensionless electromagnetic and heat conduction equations, together with their boundary and initial conditions, here represented by the system of Eqs. (11)–(15), were solved by using an iterative and conventional finite-differences method [32]. The numerical procedure is based on the following steps:

1. Recognizing that Eq. (11) is complex because its right-hand side includes, as a factor, the imaginary number i, we separate for each region the electrical current density φ, in a real part, φR, and an imaginary part φI, through the relationship $\varphi=\varphi R+i\varphi I$. After this, the resulting equation is discretized together with the boundary conditions (13) and (14) by using central differences. In this form, we can construct a matrix system which can be solved with the aid of the Gauss elimination method.
2. On the other hand, the corresponding equation for the thermal model given by Eq. (12) together with the boundary and initial conditions (13)–(15) requires a different treatment. In this case, the equations represent a non-stationary problem and therefore, the numerical procedure is based on the well-known Crank–Nicolson method that is a finite-difference method widely used for numerically solving the heat equation. In this manner, we obtain a tridiagonal matrix which is solved by using the tridiagonal matrix algorithm (TDMA), also known as the Thomas algorithm.
3. Finally, we introduce the following iterative scheme: considering a uniform profile for the temperature, we solve the electrical current density. In this manner, we can obtain the modulus or absolute value of this function. Introducing the above result into Eq. (12), we obtain the first nonuniform temperature profile. Again, we can obtain a new current density and the foregoing procedure is repeated until a convergence criterion has been fulfilled. Normally, this criterion is based on comparing the temperature and current density profiles. To validate our numerical solution, we compare the results with those of an analytic solution of the system. For the case when $\kappa=0$, an analytic solution can be obtained, as described in the Appendix.

3. Results

3.1. Effect of α

The value of the fractal dimension α was varied, in the range [0,1], in order to observe its effect on the current density and the temperature distributions through the porous medium. Even though the values $\alpha=0$ and $\alpha=1$ are not fractional, they were included in the results as mathematical limits corresponding to Euclidean spaces described by Cartesian and cylindrical coordinates, respectively.

Figs. 2 and 3 show the transient temperatures for different values of the fractal dimension α. Fig. 2 displays the dimensionless tem-

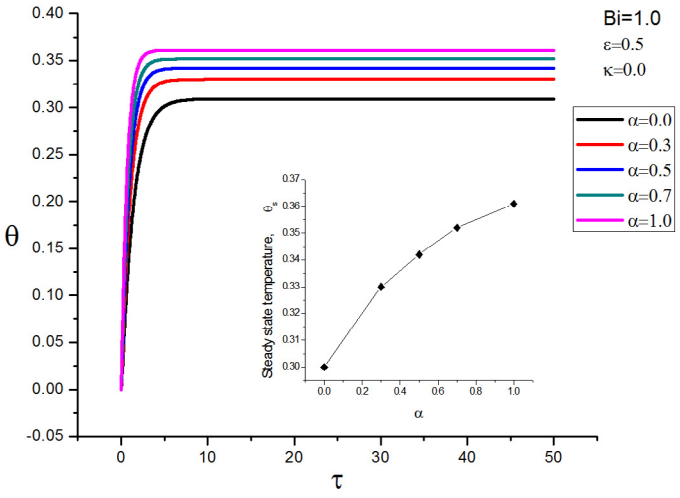

Fig. 2. Transient dimensionless temperatures at the center of the porous medium for different values of the fractal dimension. Results computed from the uncoupled model, $\kappa=0$.

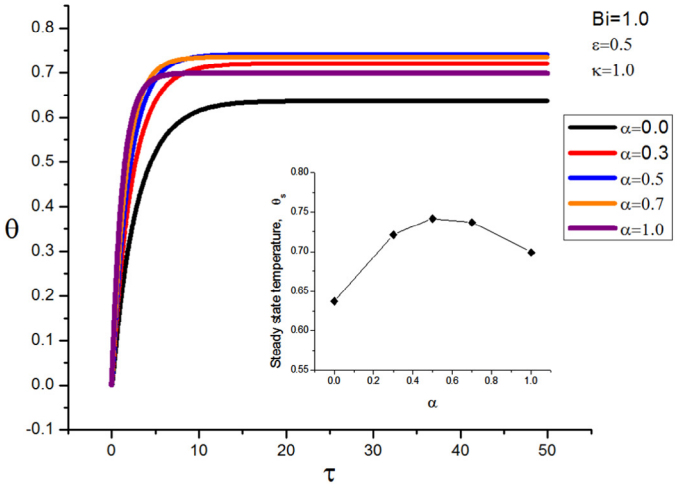

Fig. 3. Transient dimensionless temperatures at the center of the porous medium for different values of the fractal dimension. Results computed from the coupled model, $\kappa=1$.

perature at the center of the porous medium from the uncoupled model ($\kappa = 0$); clearly, all solution curves for fractional values of α lie between the Euclidean limits ($\alpha = 0$, $\alpha = 1$). It is also observed that the transient response is shorter as the fractal dimension increases. This makes sense since the anisotropy of the medium in the radial direction decreases with increasing the fractal dimension, thus enhancing the diffusion heat transfer process. Conversely, as the fractal dimension is reduced the heat transfer is weakened. Also, it should be noted that the steady state temperatures grow with the fractal dimension in a non-linear fashion; this is depicted in the inset of Fig. 2.

Fig. 3 shows the results from the coupled model ($\kappa = 1$). As in the previous case, the duration of the transient response of temperature decreases with increasing the fractal dimension. However, unlike the uncoupled model, the steady state temperature, θ_s, reaches a maximum value at $\alpha = 0.5$, see inset in Fig. 3. In all cases the steady temperature reached in the coupled case is higher due to the increment of the resistivity with temperature and therefore the increase of the heat generated by Joule's effect.

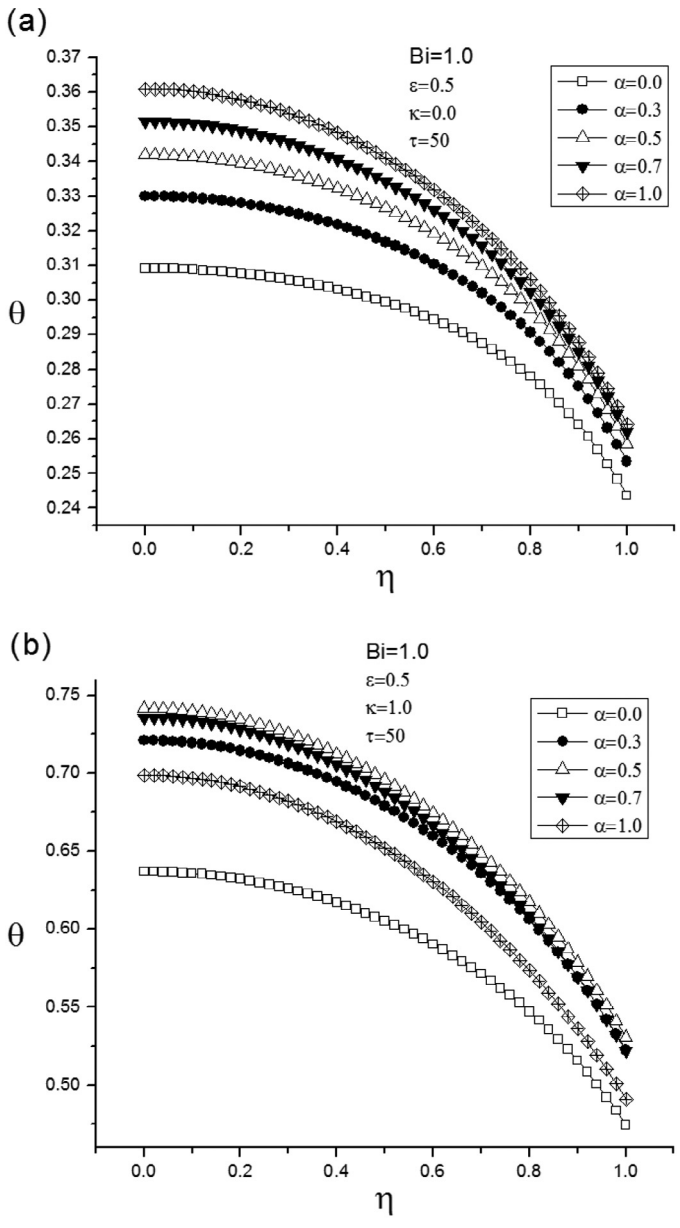

Fig. 4. Dimensionless temperature profiles for different values of the fractal dimension: (a) uncoupled model, $\kappa = 0$; (b) coupled model, $\kappa = 1$.

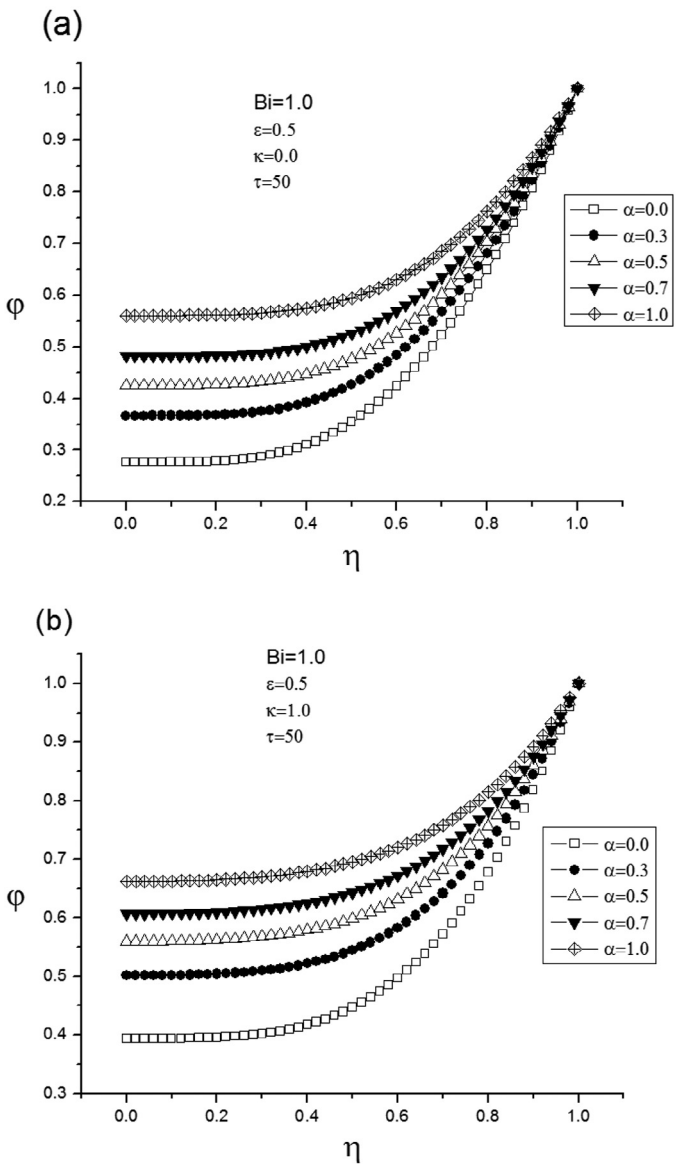

Fig. 5. Dimensionless current density distribution for different values of the fractal dimension: (a) uncoupled model, $\kappa = 0$; (b) coupled model, $\kappa = 1$.

Fig. 4 shows the dimensionless temperature profiles at steady state for different values of α. For $\kappa = 0$ the temperature profiles lie in between the limiting curves for the Euclidean cases $\alpha = 0$ and $\alpha = 1$. Clearly, the fractal dimension affects the temperature distribution; the profiles are progressively and uniformly displaced upwards as α approaches unity. Consequently, the top curve of temperature corresponds with $\alpha = 1$. Nevertheless, an unexpected behavior is observed in the results from the coupled model. In this case, the temperature profiles are displaced upwards as α is increased from 0 to values close to 0.5, then, the profiles are displaced downwards as α increases up to one.

Fig. 5 depicts the relationship between the distribution of dimensionless current density and the fractal dimension at steady state. For both the coupled and uncoupled models, the electromagnetic wave penetrates more deeply into the medium as α increases; the skin effect is accentuated for α values tending to zero since the anisotropy of the medium in the radial direction increases with

decreasing α. The influence of the κ parameter is to re-distribute the current density in the conductive medium. Higher current densities are predicted from the coupled model ($\kappa = 1$) that takes into account the changes of resistivity of the porous medium with temperature.

3.2. *Effect of* κ

In order to isolate the effect of the coupling parameter (κ), numerical results were obtained from the coupled ($\kappa = 1$) and uncoupled models ($\kappa = 0$) keeping the value of the fractal dimension, $\alpha = 0.5$, constant.

Fig. 6 illustrates the coupling parameter effect on the duration of the transient state and on the maximum temperature at the steady state. In the case $\kappa = 1$, the resistivity of the medium varies linearly with temperature; thus, when resistivity increases the generated heat increases as well and the steady state temperature predicted by the coupled model is higher than that for $\kappa = 0$. On the other hand, for the uncoupled model, the duration of the transient state is shorter than that from $\kappa = 1$. This is because the heat generation term for $\kappa = 0$ remains constant and smaller compared with the coupled model.

Figs. 7 and 8 show the effect of the coupling parameter κ on the shape and location of the current density profiles and temperature during transients. As expected, for the uncoupled model, the dimensionless temperature reaches lower values than those predicted from the coupled model, and the current density distribution remains invariant as shown in Fig. 7a. In contrast, when the parameter $\kappa = 1$, the medium is heated up and a redistribution in current density is predicted due to local changes in resistivity with temperature, see Fig. 7b. The influence of the κ parameter on the temperature profiles is clearly shown in Fig. 8; for both cases $\kappa = 0$ and $\kappa = 1$, the profiles are progressively and uniformly displaced upwards as time approaches the steady-state.

The heat transfer from the porous medium to the environment can be expressed as follows:

$$\dot{q} = h(T - T_\infty) \tag{16}$$

or in dimensionless form

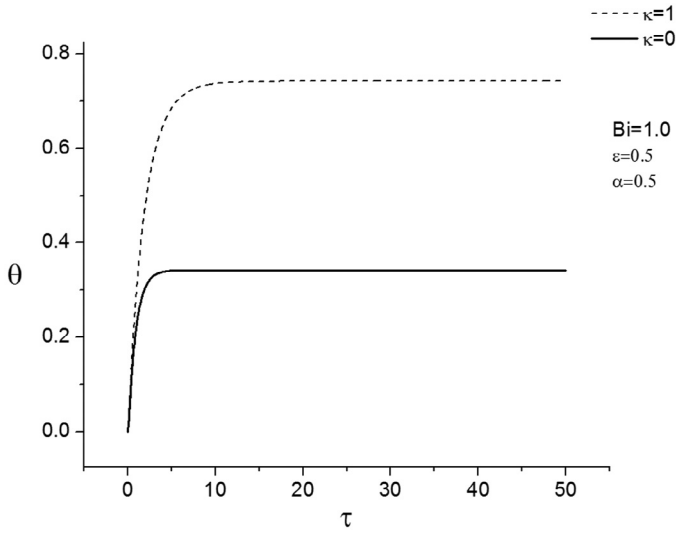

Fig. 6. Effect of κ parameter on transient dimensionless temperatures at the center of the porous medium.

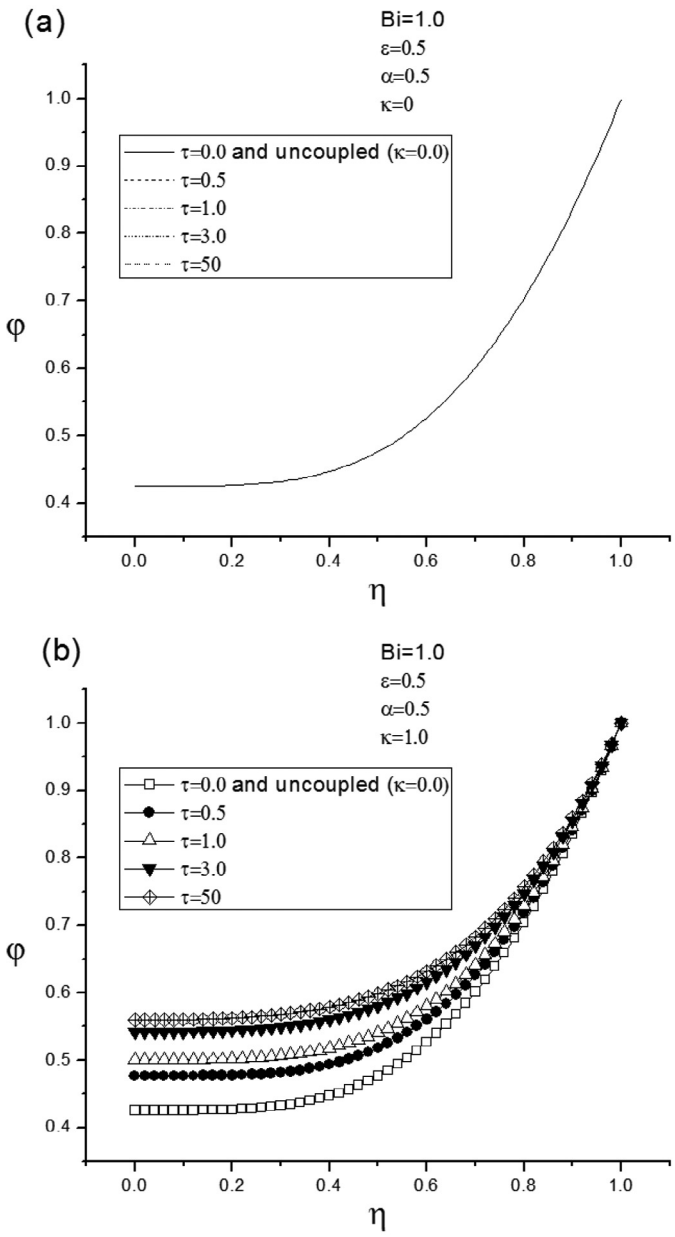

Fig. 7. Evolution in time of the dimensionless current density distribution: (a) uncoupled model, $\kappa = 0$; (b) coupled model, $\kappa = 1$.

$$\frac{\dot{q}}{h\Delta T_c} = \theta. \tag{17}$$

This expression tells us that the rate of heat transfer is, in fact, the dimensionless temperature at the surface. Fig. 9 shows the relationship between the surface temperature at steady state and the fractal dimension. For the uncoupled model, the highest rate of heat transfer occurs for the Euclidean limit $\alpha = 1$ for which, as mentioned above, there is no anisotropy in the radial direction. It is worthy to note that the nonlinear trend of the surface temperature versus α is similar to that shown in the inset of Fig. 2. For the coupled case $\kappa = 1$, the dependence of the surface temperature as a function of α reveals a parabolic-like trend with a maximum for $\alpha = 0.5$, see Fig. 10. According to Fig. 4b, this parabolic behavior would be similar at any position along the η coordinate. This is confirmed, for instance, by the plot in the inset of Fig. 3. This non-monotonic behavior is intriguing and unexpected. Clearly, in order

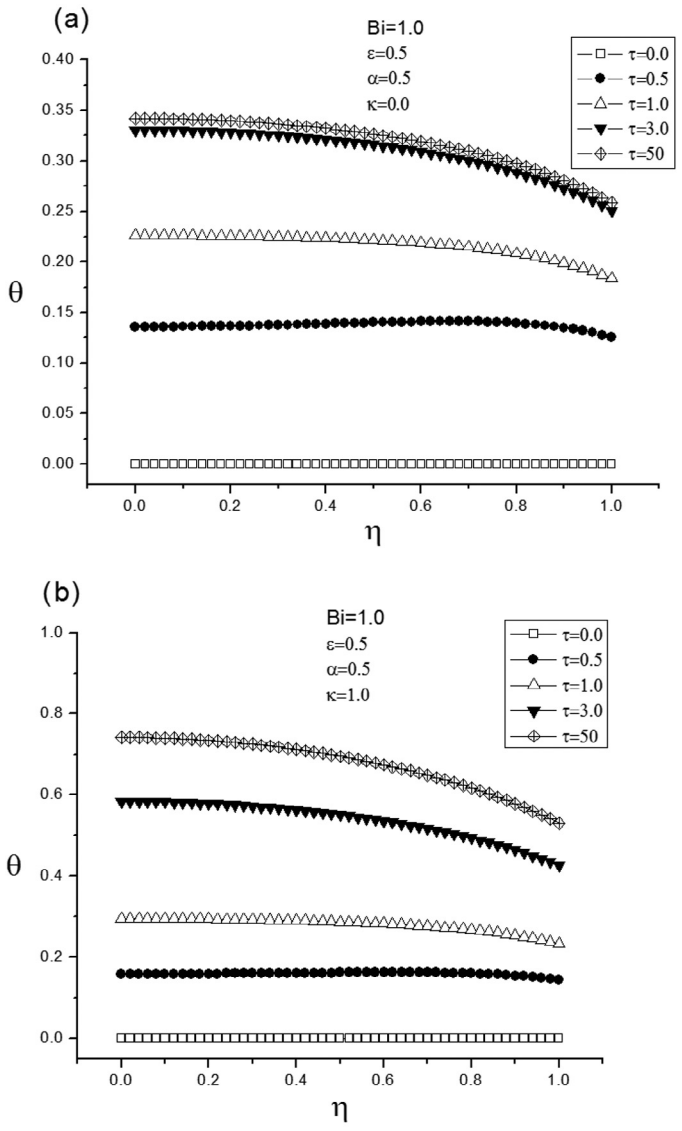

Fig. 8. Temporal evolution of the temperature profile during transient state at the center of the conductive medium: (a) uncoupled model, $\kappa = 0$; (b) coupled model, $\kappa = 1$.

to validate this trend, comparisons of the prediction with experimental data would have to be conducted. To our knowledge, such data do not exist in the literature. We thus have to defer such validation for the future. In the following section we offer a physical interpretation of this behavior.

4. Concluding remarks and discussion

A nonlinear space-fractional model that describes the combined effect of heat transfer and transmission of an electromagnetic wave through an anisotropic medium was studied. The influence of two key parameters was revealed from numerical simulations. The fractal dimension, denoted by the parameter α, was varied as $\alpha = (0.0, 0.3, 0.5, 0.7, 1.0)$; where the values $\alpha = 0.0$ and $\alpha = 1.0$ refer to Euclidean limits in Cartesian and cylindrical coordinates, respectively. The parameter κ was introduced to couple ($\kappa = 1$)/uncouple ($\kappa = 0$) the thermal and electromagnetic models. Although all results were obtained in dimensionless terms, predictions could be obtained for a real material if the values of the physical properties are known.

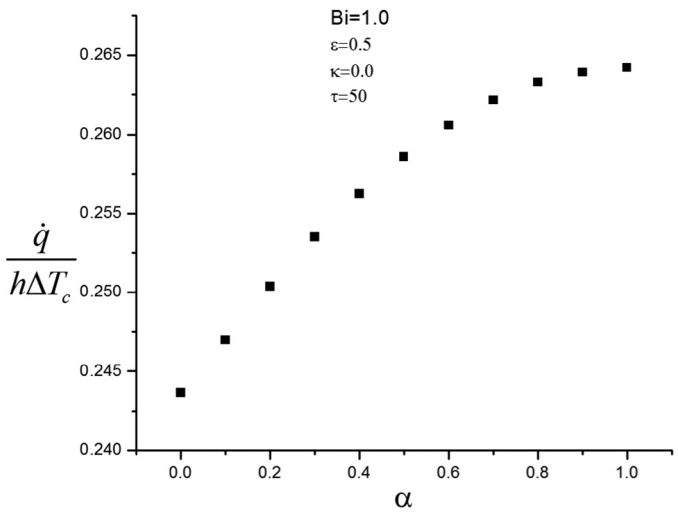

Fig. 9. Dimensionless heat transfer to the environment as a function of the fractal dimension from the uncoupled model.

The relevant results are summarized as follows:

1. Transient state
   - The dimensionless current density distribution remains invariant for the uncoupled model. However, for $\kappa = 1$ the current density is redistributed due to local changes in resistivity with temperature.
   - The duration of the transient response of temperature decreases progressively with increasing α; this behavior is observed in both cases $\kappa = 0$ and $\kappa = 1$. This result is expected since the anisotropy of the medium in the radial direction decreases with increasing α.
2. Steady state
   - The current density profiles from coupled and uncouple models show that the depth penetration of the electromagnetic wave increases with α.
   - When α decreases toward zero, the anisotropy of the medium becomes increasingly strong and the skin effect in the conductor is accentuated.

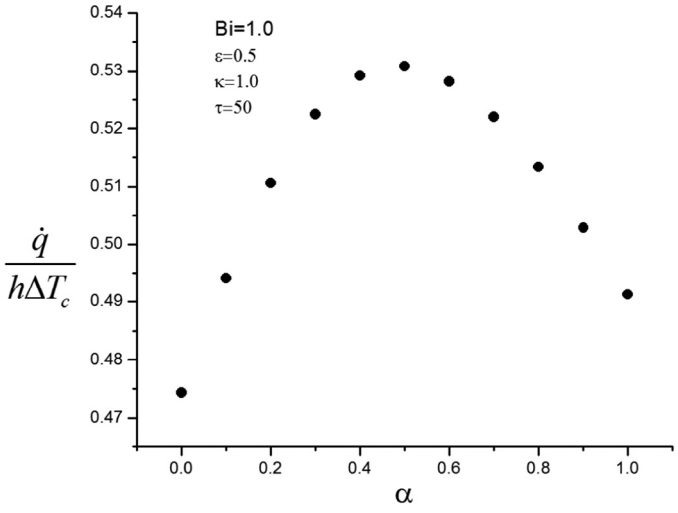

Fig. 10. Dimensionless heat transfer to the environment as a function of the fractal dimension from the coupled model.

- When the heat and wave equations are uncoupled, the temperature at steady state increases monotonically with α reaching a maximum at $\alpha = 1$; this behavior is consistent along the radial direction of the conductor.
- Surprisingly, when $\kappa = 1$, the temperature at any location along the radial axis follows a parabolic-like trend with a maximum at $\alpha = 0.5$.

Clearly the fractal dimension α plays an important role in the transmission of electromagnetic waves. According to the used formalism, α represents a parameter by which the complexity of an anisotropic medium can be quantitatively measured and modeled in a simple way. In other words, the non-local property of the fractal Laplacian allows to model the dynamics of complex processes such as heat/electromagnetic-wave transmission through a medium with long-range interactions. Our simulations reveal that α strongly affects the distribution and shape of the current density profiles as well as the heat conduction process related to the current transmission. In summary, our numerical results can be interpreted from two perspectives:

(i) Firstly, in physical terms, as α increases from 0 to 1, the degree of anisotropy of the medium decreases, and consequently the diffusion heat transfer process is enhanced while the skin effect is accentuated. Alternatively, a physical interpretation can be drawn by analyzing the form of the fractal Laplacian at the limiting values of α. This operator appears in both the heat conduction Eq. (12) and the wave equation deduced from Maxwell's equations [24],

$$\nabla^2 \lambda \vec{J} = \frac{\partial^2 \lambda \vec{J}}{\partial r^2} + \frac{\alpha}{r}\frac{\partial \lambda \vec{J}}{\partial r} = \mu\left(\frac{\partial \vec{J}}{\partial t} + \gamma \frac{\partial^2 \lambda \vec{J}}{\partial t^2}\right). \tag{18}$$

Hence, the scheme proposed here models the process of coupling-uncoupling of Eqs. (12) and (18). For $\alpha = 0$, the Laplacian reduces to $\nabla^2 = \frac{\partial^2}{\partial r^2}$, which indicates, in accordance with Eq. (12), a purely diffusive process.

On the other hand, when $\alpha = 1$, the Laplacian becomes:

$$\nabla^2 = \frac{\partial^2}{\partial r^2} + \frac{1}{r}\frac{\partial}{\partial r}. \tag{19}$$

In addition to the first diffusive term in the right hand side of Eq. (19), the second term can be associated with a convective process. So, in the range $0 \le \alpha \le 1$, Eq. (12) represents a family of fractional equations whose solutions have intermediate behaviors in between a convection-diffusion equation ($\alpha = 1$) and a purely diffusion equation ($\alpha = 0$). Note that, in all cases, a non-linear source of heat due to Joule's effect also affects the solutions.

In the same manner, the fractional wave Eq. (18) can be interpreted as an intermediate state between a wave equation with a linear convection term ($\alpha = 1$) and a classical wave equation ($\alpha = 0$). Similar arguments and interpretations have been previously discussed by others [33,34].

(ii) Secondly, in mathematical terms, the gradual increase of α from 0 to 1 implies a gradual shift from one Cartesian coordinate system to a cylindrical one, and in between these two Euclidean limits there are an infinite number of fractional intermediate cases. From a purely mathematical point of view, it is not trivial to predict the behavior of such fractional states. Our numerical results are useful to gain some insight about the nature of the solution of these fractal equations.

In our opinion, all above numerical results need to be evaluated experimentally on anisotropic conductors as a prior step to develop potential applications. As future work, we plan to include two more fractal dimensions to quantify anisotropies in the angular (Φ) and longitudinal (z) directions of a cylindrical conductor, which may result in a more realistic description. Our model could also be used to study other exotic materials; for instance, the behavior of a negatively coupled system ($\kappa = -1$, resistivity decreases with temperature) could be studied.

Acknowledgements

We thank Prof. A. Balankin for fruitful discussions. The generous support of CONACyT-Mexico through its SENER-HIDROCARBUROS program (grant number: 143927) is greatly acknowledged.

Appendix

Analytical solutions for the uncoupled electric model ($\kappa = 0$)

When κ is set to zero, the thermal and electromagnetic effects are uncoupled. Therefore Eq. (11) can be written as:

$$\frac{d^2\varphi}{d\eta^2} + \frac{\alpha}{\eta}\frac{d\varphi}{d\eta} - \frac{2i}{(1+\kappa\theta)\varepsilon^2}\varphi = 0, \tag{A1}$$

subject to:

$$\text{at} \quad \eta = 0: \quad \varphi = \text{finite}, \tag{A2}$$

$$\text{at} \quad \eta = 1: \quad \varphi = 1. \tag{A3}$$

Eq. (A1) is, in fact, a transformed version of the Bessel differential equation given by Bowman [35]. Thus, after taking into account the conditions (A2) and (A3), the particular solution of Eq. (A1) in a Euclidean space, i.e. $\alpha = 1$, is:

$$\varphi(\eta) = \frac{J_0\left(\frac{(1-i)}{\varepsilon}\eta\right)}{J_0\left(\frac{(1-i)}{\varepsilon}\right)}, \quad 0 < \eta \le 1 \tag{A4}$$

The curve from Eq. (A4) is shown in Fig. A1. This curve represents an upper bound of the possible solutions of Eq. (A1). Although in general $\alpha > 0$, as defined in [18] and [31], it is useful to find a

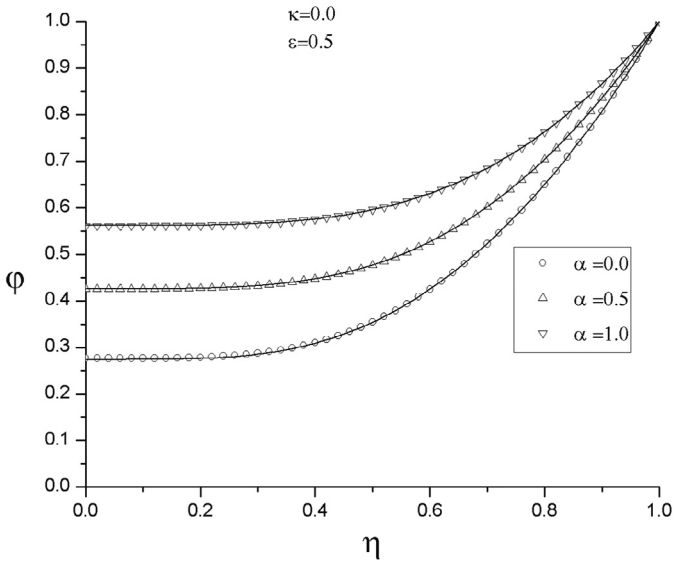

Fig. A1. Dimensionless current density distribution φ as a function of the radial coordinate η for three values of the parameter α. Open symbols: numerical simulations. Solid lines: analytical solutions.

particular solution of Eq. (A1) for $\alpha = 0$. The solution can readily be found:

$$\varphi(\eta) = cosh\left(\frac{(1+i)}{\varepsilon}\eta\right) sech\left(\frac{(1+i)}{\varepsilon}\right), \quad 0 \le \eta \le 1 \tag{A5}$$

This solution, also shown in Fig. A1, corresponds to a lower bound solution of the general case. Thereby, the particular solutions of Eq. (A1), for fractional α, lying in between the upper and lower bound solutions, are of the form

$$\varphi(\eta) = \frac{n^{\frac{1}{2}\frac{\alpha}{2}} J_n\left(\frac{(1-i)}{\varepsilon}\eta\right)}{J_n\left(\frac{(1-i)}{\varepsilon}\right)}, \quad 0 < \eta \le 1 \tag{A6}$$

where $n = \frac{\alpha - 1}{2}$.

Clearly, as shown in Fig. A1, the agreement between the numerical and analytical solutions for $\kappa = 0$ is excellent. This comparison validates, to some extent, our finite difference scheme.

Nomenclature

Variable	Name, units
Bi	Biot number $Bi = \frac{hR}{k_{ef}}$
c	Specific heat $\left[\frac{J}{Kg°C}\right]$
D	Total fractal dimension
h	Convective coefficient $\left[\frac{W}{m^2\,°C}\right]$
I	Electrical current $[A]$
i	Imaginary number $\sqrt{-1}$
J_s	Current density $\left[\frac{A}{m^2}\right]$
J_0, J_n	Bessel functions
k	Thermal conductivity $\left[\frac{W}{m°C}\right]$
q	Generated heat $\left[\frac{W}{m^3}\right]$
R	Conductor radius $[m]$
r	Radial coordinate $[m]$
T	Temperature [°C]
ΔT_c	Characteristic temperature [°C]
t	Time $[s]$
z	Axial coordinate $[m]$

Greek symbols

α	Fractal dimension in radial direction
γ	Electric permittivity $\left[\frac{F}{m}\right]$
δ	Skin depth $\delta = \sqrt{\frac{2\lambda}{\omega\mu}}[m]$
ε	Skin parameter
ϕ	Temperature coefficient $\left[\frac{1}{°C}\right]$
φ	Dimensionless current density
η	Dimensionless radial coordinate
κ	Coupling parameter
λ	Electric resistivity $[\Omega m]$
μ	Magnetic permeability $\left[\frac{J}{A^2 m}\right]$
θ	Dimensionless temperature
ρ	Density $\left[\frac{Kg}{m^3}\right]$
τ	Dimensionless time 20
ω	Angular frequency $\left[\frac{rad}{s}\right]$

Subscripts

∞	Environmental conditions
R	Evaluated at conductor surface
s	At steady state
Tot	Total

References

[1] D. Cafagna, Fractional calculus: a mathematical tool from the past for present engineers [Past and present], IEEE Ind. Elect. Mag. 1 (2007) 35–40.
[2] H. Nasrolahpour, Time fractional formalism: classical and quantum phenomena, Prespacetime J. 3 (2012) 99–108.
[3] M. Caputo, Diffusion with space memory modeled with distributed order space fractional differential equations, Ann. Geophys. 46 (2003) 223–234.
[4] M. Rahimy, Applications of fractional differential equations, App. Math. Sci. 4 (2010) 2453–2461.
[5] M. Caputo, Linear models of dissipation whose Q is almost frequency independent, Geophys. J. Royal Astr. Soc. 13 (1967) 529–539.
[6] S.I. Muslih, O.P. Agrawal, Riesz fractional derivatives and fractional dimensional space, Int. J. Theor. Phys. 49 (2010) 270–275.
[7] M. Riesz, L'integrale de riemann-liouville et le probleme de cauchy, Acta Math. 81 (1949) 1–223.
[8] N. Laskin, Fractional Schrödinger equation, Phys. Rev. E 66 (2002) 056108.
[9] M. Weilbeer, Efficient Numerical Methods for Fractional Differential Equations and Their Analytical Background, Papierflieger, Germany, 2006.
[10] K.B. Oldham, J. Spanier, The Fractional Calculus, Academic Press, New York, 1974.
[11] W.E. Olmstead, R.A. Handelsman, Diffusion in a semi-infinite region with nonlinear surface dissipation, SIAM Rev. 18 (1976) 275–291.
[12] R. Bagley, P.J. Torvik, A theoretical basis for the application of fractional calculus to viscoelasticity, J. Rheol. 27 (1983) 201–2110.
[13] R.J. Marks, M.W. Hall, Differintegral interpolation from a bandlimited signals samples, IEEE T. Acoust. Speech 29 (1981) 872–877.
[14] S.I. Muslih, D. Baleanu, Fractional multipoles in fractional space, Nonlin. Anal. Real World Appl. 8 (2007) 198–203.
[15] A.S. Balankin, B. Mena, J. Patiño, D. Morales, Electromagnetic fields in fractal continua, Phys. Lett. A 377 (2013) 783–788.
[16] Z.S. Wang, B.W. Lu, The scattering of electromagnetic waves in fractal media, Wave. Random Media 4 (1994) 97–103.
[17] G.E. Archie, The electrical resistivity log as an aid in determining some reservoir characteristics, Trans. AIME 146 (1942) 54–62.
[18] M. Zubair, M.J. Mughal, Q.A. Naqvi, An exact solution of the cylindrical wave equation for electromagnetic field in fractional dimensional space, Prog. Electromagn. Res. 114 (2011) 443–455.
[19] M. Zubair, M.J. Mughal, Q.A. Naqvi, The wave equation and general plane wave solutions in fractional space, Prog. Electromagn. Res. Lett. 19 (2010) 137–146.
[20] M. Zubair, M.J. Mughal, Q.A. Naqvi, A.A. Rizvi, Differential electromagnetic equations in fractional space, Prog. Electromagn. Res. 114 (2011) 255–269.
[21] M. Zubair, M.J. Mughal, Q.A. Naqvi, On electromagnetic wave propagation in fractional space, Nonlinear Anal.-Real 12 (2011) 2844–2850.
[22] L. Dongqing, Electrokinetics in Microfluidics, Elsevier, Netherlands, 2004.
[23] K. Agrawal, Industrial Power Engineering and Applications Handbook, Newnes, Boston, USA, 2001.
[24] O. Chávez, F. Méndez, Conjugate heat transfer in a bimetallic conductor with variable electric resistivity, Appl. Therm. Eng. 31 (2011) 3420–3427.
[25] F.H. Stillinger, Axiomatic basis for spaces with noninteger dimension, J. Math. Phys. 18 (1977) 1224–1234.
[26] X.F. He, Anisotropy and isotropy: a model of fraction-dimensional space, Solid State Commun. 75 (1990) 111–114.
[27] X.F. He, Excitons in anisotropic solids: the model of fractional-dimensional space, Phys. Rev. B 43 (1991) 2063–2069.
[28] X.F. He, Fractional dimensionality and fractional derivative spectra of interval optical transitions, Phys. Rev. B 42 (1990) 751–756.
[29] C. Smithells, Metals Reference Book, Butterworth, New York, USA, 1976.
[30] C. Moosbrugger, ASM Ready Reference: Electrical and Magnetic Properties of Metals, ASM International, New York, USA, 2000.
[31] C. Palmer, P. Stavrinou, Equations of motion in a non-integer-dimensional space, J. Phys. A 37 (2004) 6987–7003.
[32] M. Ozisik, Finite Difference Methods in Heat Transfer, CRC Press, Boca Raton, USA, 1994.
[33] L. Vazquez, J.J. Trujillo, M.P. Velasco, Fractional heat equation and the second law of thermodynamics, Fract. Calc. Appl. Anal. 14 (2011) 334–342.
[34] L. Vazquez, From Newton's equation to fractional diffusion and wave equations, Adv. Differ. Equ.-NY (2011) 169421.
[35] F. Bowman, Introduction to Bessel Functions, Dover, New York, USA, 1958.